

Robust operation of a universal set of logic gates for quantum computation using adiabatic population transfer between molecular levels

Cian Menzel-Jones^{1,*} and Moshe Shapiro^{1,2,3}¹*Department of Physics and Astronomy, The University of British Columbia, Vancouver, British Columbia, Canada, V6T 1Z3*²*Department of Chemistry, The University of British Columbia, Vancouver, British Columbia, Canada, V6T 1Z3*³*Department of Chemical Physics, The Weizmann Institute, Rehovot 76100, Israel*

(Received 26 July 2006; published 7 May 2007)

We present a robust construction of a set of logic gates operating on a system of qubits encoded in the rovibrational eigenstates of an Na₂ molecule using the optical adiabatic population transfer (APT) phenomenon. We demonstrate the operation of a complete universal gate set for quantum computation on a two-qubit system with gate fidelities approaching 99.99%. Like other APT-based processes, the method is robust against substantial fluctuations in the intensity of the laser pulse. Our construction is easily scalable to deal with a larger number of qubits. With the aid of the set of gates thus shown we may construct pulse sequences for a wide class of quantum logic operations. We also show how to produce a representation of Bell states from a representation of product states with essentially perfect fidelity. Our scheme can be realized in all diatomic and polyatomic molecules that possess easily accessible and well characterized excited electronic states.

DOI: [10.1103/PhysRevA.75.052308](https://doi.org/10.1103/PhysRevA.75.052308)

PACS number(s): 03.67.Lx, 33.80.-b

I. INTRODUCTION

It is well known that all logic circuits of interest to quantum computations can be realized by a sequence of a small set (“gate set”) of one-qubit and two-qubit logic gates [1]. Such a “universal” gate set is composed of the one-qubit phase shifter, the Hadamard gate, and the two-qubit controlled-NOT (CNOT) gate. There have been many proposals of implementing these and other universal gate sets on various quantum systems [1].

In the past a number of authors have considered using the vibrational modes of molecules as platforms for quantum computations. Most of these papers [2–7] have derived the pulses that produce the desired logic gate numerically, using optimal control theory (OCT) [8–10]. The drawback of this approach is that the pulses thus produced are critically dependent on the exact knowledge of the potential-energy surface(s) on which the nuclei move. Such knowledge is usually not accurate enough for high fidelity operations. In addition, the pulses obtained using OCT are extremely sensitive to the pulse details. For example, like in the use of a π pulse to induce population exchange between two levels, the OCT derived pulses are extremely sensitive to the *pulse area*. Moreover, the OCT derived pulses are sensitive to the exact *phase chirp* and *pulse shape*. Since in real experiments it is very difficult to produce pulses whose parameters are accurate to a fraction of a percent, as dictated by the quantum computations requirements, the method is very difficult, if not impossible, to apply in practice.

Adiabatic turn-on and turn-off of an interaction appears to be a natural direction for performing operations needed for quantum computation. Recently, several groups have proceeded in this general direction and have suggested using “adiabatic quantum computing” [11–16] and “holonomic computing” [17–20], for performing logic manipulations in various systems.

In this paper we take a seemingly easier adiabatic approach, relying on adiabatic population transfer (APT) between sets of three and four quantum levels. The main idea is to build *all* the gates mentioned above via the in-tandem applications of adiabatic passage (AP) [21–26] steps. We show using a system of qubits encoded in the rovibrational eigenstates of the sodium dimer molecule (Na₂) that the method fidelities approach the presumed fault-tolerant threshold value of 99.99%.

In contrast to the numerically derived OCT-based pulses, APT is very robust. Once the theoretically specified order of delay times and *adiabatic conditions* $\Omega_i \tau_i \gg 1$, where Ω_i is an effective Rabi frequency of the *i*th pulse, and τ_i is its duration, are met, APT is rather insensitive to the exact values of Ω_i and τ_i and other pulse parameters [21,22,27,28]. However, in our case, since we use a nondegenerate encoding for the qubits, the duration τ for each pulse will be precisely defined such that the optical phase accumulations of the states can be worked into our scheme. With the pulse duration specified, this will still allow for significant variation in the pulse intensities dictated by the adiabatic conditions. Moreover, because APT is a generic scheme it does not change in essence from one set of levels to another. In this application, it involves resonant transitions between a small (3 or 4) number of levels, the input for the universal gate set construction consists of a few dipole matrix elements, which, if necessary, can be extracted experimentally. No theoretical knowledge of an entire potential-energy surface is necessary.

The APT based logic gates we demonstrate rely mainly on introducing the pulses in the right sequence and maintaining the electric field’s amplitudes and their analytically derived phases in accordance with the requirements of the logic operation at hand. Below we demonstrate both the great stability and the near-perfect gate fidelities we achieve in the one- and two-qubit Na₂ systems. Because of the universality, this method can be implemented in other quantum gates not explicitly considered here and be readily scaled up to treating multi (≥ 3)-qubit systems [24].

*Electronic address: cianmj@physics.ubc.ca

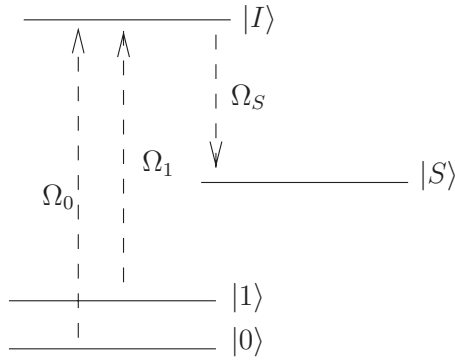


FIG. 1. Interaction scheme for one-qubit gate operations using APT. The qubit states, $|0\rangle$ and $|1\rangle$, are coupled to an excited state $|I\rangle$ by two different laser fields. A third states, $|S\rangle$, coupled to the intermediate state $|I\rangle$ acts as a shelving or auxiliary state for the gate procedures.

II. ONE-QUBIT GATES

A. Single qubit adiabatic population transfer

Our general strategy is based on adiabatic passage phenomena. One of the best known applications of AP, called stimulated Raman adiabatic passage (STIRAP) [21,22,27,28], allows for populations to be transferred from an initial bound state $|0\rangle$ to a final state $|1\rangle$ in a complete fashion. The method is based on performing a stimulated Raman process via a third level $|I\rangle$ using two laser pulses with central frequencies in near resonance with the transitions from $|0\rangle$ to $|I\rangle$ and from $|I\rangle$ to $|1\rangle$. As shown by Bergmann and co-workers [21,22], when the lasers are turned on in a “counterintuitive” order (i.e., by first coupling $|I\rangle$ to $|1\rangle$ and then coupling $|I\rangle$ to $|0\rangle$) the population moves directly from $|0\rangle$ to $|1\rangle$ while leaving the intermediate state $|I\rangle$ empty.

Consider a single qubit in an arbitrary state given by

$$|\psi_0\rangle = \alpha|0\rangle + \beta|1\rangle \quad (1)$$

which has the typical normalization such that $|\alpha|^2 + |\beta|^2 = 1$. In performing the APT scheme, two additional nondegenerate states are introduced, as shown in Fig. 1. The first additional state, labeled $|S\rangle$, is used for temporary population shelving. It must therefore be long-lived relative to the duration of the gate operation. This is not a very restrictive requirement because our pulse durations are in the ps to ns domain. The second additional state, labeled $|I\rangle$, acts as the intermediate state in the APT population transfer scheme. Because it never gets populated, its actual lifetime is of no importance.

B. Encoding qubits on molecular energy levels

In the APT scheme, we use as the intermediate state, that must be coupled to the two other levels, a rovibrational state belonging to an electronic manifold different than that of the initial and final states. In this way we minimize the restrictions imposed by the optical selection rules. For example, transitions within the same electronic state depend on the presence of a permanent electric dipole moment which is absent for homonuclear diatomics and is confining for het-

eronuclear diatomics, whose levels couple to a given state by the $\Delta J = \pm 1$ and $\Delta v \approx \pm 1$ selection rules, where v and J label the vibrational and rotational quantum numbers, respectively [29]. More specifically, we select low-energy rovibrational levels $|v, J\rangle$ in the $B^1\Pi_u$ electronic state of Na_2 to house our intermediate levels. These states are optically accessible from nearly all of the $X^1\Sigma_g^+$ ground states, and have transition dipole moments, $B \rightarrow X$, that are less dependent on internuclear distance than other electronic surfaces (e.g., $A^1\Sigma_u^+$) [30].

Because both the shelving state and the states used to store the qubits (“qubits states”) should be stable against decoherences due to spontaneous emission, we use for these states low-lying rovibrational eigenstates in the ground electronic state, $X^1\Sigma_g^+$, of the Na_2 molecule. The average lifetimes for spontaneous emission in the infrared may be as long as a few milliseconds (ms) [31,32], allowing plenty of time for the completion of all logic operations of interest.

We have chosen to use a diatomic molecule so as to avoid an additional coupling between qubit states and nonqubit states belonging to other normal modes of vibration of the same molecule, a complication encountered by other groups using polyatomic molecular states coupled by broad band pulses [7].

C. Numerical simulations

The viability of the following schemes are demonstrated by performing a number of simulations of one- and two-qubit systems encoded in a Na_2 molecule. In all cases our simulations are derived from a numerical solution of the Schrödinger equation using a molecular set of energy levels, coupled through typical electric-dipole matrix elements by pulses satisfying the adiabatic condition. We present our results in the interaction representation, thus omitting the dynamical phase of each of the states from the figures. These phases can each be monitored and integrated into these schemes by the appropriate timing and durations of the laser pulses. In addition to establishing the very high fidelity rates of our schemes, our simulations also serve to obtain realistic estimates for the durations of the various gate operations. For all cases studied we have conservatively considered laser powers of approximately 10 MW/cm^2 and pulse durations of 100 ps, which satisfy the adiabatic conditions for typical optically allowed molecular transitions.

The fidelity of each gate is computed as the overlap between the expected wave function, $|\Phi\rangle$, and that obtained numerically, $|\phi_n\rangle$, at the conclusion of each gate operation. We show that the fidelities for the $\pi/8$ phase (T), Hadamard, and CNOT gates, which make up a universal and fault-tolerant basis for quantum computation [33], are all essentially unity. Note, these gates comprise the “standard” four-element universal gate set: The π -phase shifter (S), T , Hadamard, and CNOT gates. Since S is related to T it suffices to demonstrate the implementation of T .

For the single qubit operations we take the $v=1, J=1$ state in $B^1\Pi_u$, $|B, 1, 1\rangle$, as our intermediate level. By the optical selection rules we know that this will couple strongly to at least the three rovibrational levels in $X^1\Sigma_g^+$, $|X, v=0, J=0\rangle$, $|X, v=0, J=2\rangle$, and $|X, v=2, J=0\rangle$ which we use to

represent the $|0\rangle$, $|S\rangle$, and $|1\rangle$ states, respectively. This restrictive coupling between eigenstates allows us to avoid decoherences during our gate operations due to off-resonant couplings between other nonparticipating states. The relevant Franck-Condon factors are calculated using a discrete-variable representation method which has been validated using previously published calculations [34,35].

We note that in some of the simulations presented below where a chain of elementary APT processes is constructed to yield a complex logical operation, the pulse that terminates one elementary APT process may in fact be identical in all aspects to the pulse that initiates the subsequent step. As we show below, in such cases we can conjoin these two pulses into one pulse. The use of such conjoined pulse chains simplifies the experimental setup and saves on gate operation times.

D. Phase gates

The standard matrix representation of a one-qubit phase gate is given by

$$R(\phi) = \begin{pmatrix} 1 & 0 \\ 0 & e^{i\phi} \end{pmatrix}.$$

$R(\phi)$ acts on the initial state ψ_0 of Eq. (1) by adding a relative phase ϕ to the phase of $|1\rangle$, leading to an output state

$$|\psi_f\rangle = \alpha|0\rangle + e^{i\phi}\beta|1\rangle. \quad (2)$$

We make use of the fact that population transfer between states using adiabatic passage adds a controllable phase to the final state. An obvious implementation of this fact is to use two consecutive but independent applications of APT involving the shelving state $|S\rangle$ as previously shown in [23,24]. In the first step, two laser pulses with *real* Rabi frequencies $\Omega_1(t)$ and $\Omega_S(t)$ (see Fig. 1), tuned to be in resonance with the $|1\rangle-|I\rangle$ and $|I\rangle-|S\rangle$ transitions, respectively, are used to adiabatically transfer the entire population of state $|1\rangle$ to state $|S\rangle$. In the second step, the population is transferred back from state $|S\rangle$ to state $|1\rangle$, however, this time we use a complex Rabi frequency $\Omega_S(t)=|\Omega_S(t)|e^{i\phi}$. The second pulse sequence induces the $|S\rangle \rightarrow e^{i\phi}|I\rangle \rightarrow e^{i\phi}|1\rangle$ two-photon process. The net result of both steps is to encode a phase ϕ onto state $|1\rangle$ exclusively. The complete success of this strategy is demonstrated below.

1. $\pi/8$ phase gate operation

Initializing our system to be the $|+\rangle$ one-qubit state,

$$|\psi_i\rangle = |+\rangle = \frac{1}{\sqrt{2}}(|0\rangle + |1\rangle), \quad (3)$$

a T -gate operation adds a relative phase to $|1\rangle$ such that our state goes into

$$|\psi_f\rangle = \frac{1}{\sqrt{2}}[|0\rangle + (\alpha_- + i\alpha_+)|1\rangle], \quad (4)$$

where $\alpha_{\pm} = (2 \mp 2^{1/2})^{1/2}/2$.

In Fig. 2 we present a simulation of this logic gate. As shown in panel (c) the final values obtained numerically are

exactly the desired values of Eq. (4). Thus the gate fidelity is virtually perfect! We see that as required, the first APT process, which uses the pulse sequence Ω_S and Ω_1 , completely transfers the population of state $|1\rangle$ to state $|S\rangle$. When the process is reversed and a $\pi/8$ phase is imparted to Ω_S , the population flows back to the initial state which acquires exactly a $\pi/8$ phase. It is evident from Fig. 2(a) that even with the conjoining of the two pulses between the APTs, gate fidelities in our Na_2 system remain in excess of 99.9%. The minor reduction in fidelity can be attributed to additional laser couplings between off-resonant levels in our molecule resulting in the temporary occupation of the intermediate level and the minor deviation of the imaginary part of the $|0\rangle$ coefficient from zero shown in Fig. (4).

E. Hadamard gate

One of the most useful quantum gates, commonly used to initialize entanglement within a qubit system, is the Hadamard gate represented by the matrix

$$H = \frac{1}{\sqrt{2}} \begin{pmatrix} 1 & 1 \\ 1 & -1 \end{pmatrix}.$$

The action of H on the initial state of Eq. (1) yields

$$|\psi_f\rangle = \frac{1}{\sqrt{2}}[(\alpha + \beta)|0\rangle + (\alpha - \beta)|1\rangle]. \quad (5)$$

In the last few years a number of papers have looked into the adiabatic manipulation of four-states in the so-called “tripod” system [23,36], consisting of a threefold degenerate ground state coupled to a single excited state. These papers have demonstrated the versatility of APT in controlling the tripod system to various desired final states. Here we show how to use adiabatic passage in specifically implementing the Hadamard gate on our molecular system.

An important prerequisite for the success of the adiabatic schemes for the tripod system is that each of the three degenerate states be individually addressable by the laser pulses. This means that each Rabi frequency involved must couple only one of the degenerate states to the excited “transfer” state. Additionally, these three excited levels must be sufficiently long lived to eliminate the loss of coherence via decay.

In the present application, the tripod scheme is composed of nondegenerate states. Thus the anharmonicity of the electronic potential-energy surface of the molecule is sufficient to guarantee the one-to-one correspondence between the laser frequencies and the transition frequencies, resulting in easy and accurate addressability. Considering that the typical spacings between two low-lying rovibrational eigenstates is ~ 0.001 eV, our gate operations can be done using lasers as short as picosecond (ps) pulses. This time scale is much shorter than the recorded average lifetimes of excited rovibrational levels in the ground-state electronic surface [31], allowing us to completely avoid decoherences due to spontaneous decay. However, the nondegeneracy of our states

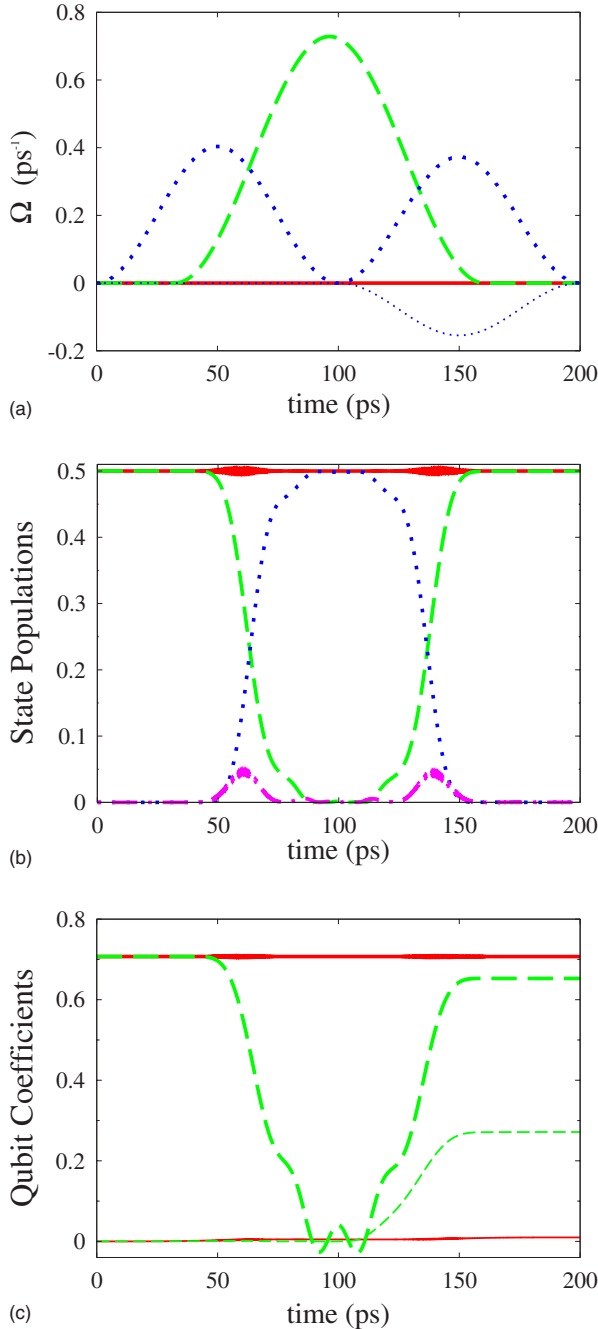


FIG. 2. (Color online) Numerical simulation of the $\pi/8$ -phase gate implemented on a one-qubit system initialized to an even superposition of the $|0\rangle$ and $|1\rangle$ qubit states. Where present, the thinner lines on the plots represent the imaginary part of the variable corresponding to that line type. All times shown are in ps. (a) Profiles of the Rabi frequencies Ω_i for each of the pulses in resonance with the $|i\rangle$ - $|I\rangle$ transitions used to carry out the gate operation. Solid line: Ω_0 . Dashed line: Ω_1 . Dotted line: Ω_S . Notice that only the last pulse contains an imaginary part due to the added phase shift. Units are 1/ps. (b) Temporal evolution of the probability amplitudes for each of the states: $|0\rangle$ (solid line), $|1\rangle$ (dashed line), $|S\rangle$ (dotted line), and $|I\rangle$ (dot-dashed line). As expected, the final populations of the $|0\rangle$ and $|I\rangle$ states are not significantly affected. (c) The real and imaginary parts of the qubit coefficients: $|0\rangle$ (solid line) and $|1\rangle$ (dashed line). The thicker upper two lines on the right-hand side of the plot represent the real parts of each state's coefficients.

also means that each level will accumulate a different dynamical phase, which did not occur in the original tripod system. Thus just as in any system using a nondegenerate qubit encoding, we must be careful to monitor each state's phase evolution and time our pulses appropriately or risk losing our high gate fidelities.

With these issues resolved, we have constructed a molecular Hadamard gate using the tripod scheme of Kis and Renzoni [23]. These researchers have shown how to perform an arbitrary rotation on two of the ground tripod states. Similar to the phase gate, their scheme uses two consecutive APT sequences characterized as

$$\Omega_0(t) = \Omega(t)\cos\chi,$$

$$\Omega_1(t) = \Omega(t)e^{i\eta}\sin\chi,$$

$$\Omega_S(t) = \Omega(t)e^{i\delta'} \quad (6)$$

with the arrangement shown in Fig. 1. By appropriately tuning the three pulsed Rabi frequencies of Eq. (6) one transforms the initial qubit state $|\psi_0\rangle$ to a final state given as

$$|\psi_f\rangle = e^{i\delta/2}(\cos\delta - i\mathbf{n} \cdot \underline{\sigma} \sin\delta)|\psi_0\rangle, \quad (7)$$

where $\underline{\sigma} = (\underline{\sigma}_x, \underline{\sigma}_y, \underline{\sigma}_z)$ with $\underline{\sigma}_i$, $i = \{x, y, z\}$ being the Pauli matrices. $\mathbf{n} = (\sin 2\chi \cos \eta, \sin 2\chi \sin \eta, \cos 2\chi)$ is a unit vector in three-dimensional (3D) space. Apart from a global phase $-\delta/2$, the above transformation constitutes a rotation of $|\psi_0\rangle$ by an angle δ about the unit vector \mathbf{n} .

The direction of the rotation axis \mathbf{n} is defined by the magnitudes and relative phases of the Rabi frequencies coupling the rotating qubit state to $|I\rangle$, given by $\Omega_0(t)$ and $\Omega_1(t)$ in Eq. (6). In contrast, the angle of rotation and global phase is determined solely by the relative difference in the phases of $\Omega_2(t)$ for the two APT processes. Thus if δ' is the same in both steps, we get $\delta=0$, and we return back to our initial state.

A simple calculation shows that the values of the above parameters required to implement a Hadamard gate are given by $\chi = \frac{3\pi}{8}$, $\eta = \pi$, and $\delta = |\delta'_1 - \delta'_2| = \pi$, where δ'_i represents the i th APT processes. Note that the global phase of the final state shown in Eq. (7), now equal to $e^{i\pi/2} = i$, gets used in constructing the Hadamard gate operation.

1. Hadamard gate operation

In Fig. 3 we show the results of simulating the one-qubit Hadamard gate starting from a single initial state ($|0\rangle$), using the Rabi frequencies as described above. As shown in panel (b) of that figure, our initial state evolves into precisely the $|+\rangle$ state of Eq. (3). As in the phase gate, changes in the timings between the two APT processes does not reduce the essentially perfect gate fidelity. As illustrated in Fig. 3(b), the first APT step takes the system into a superpositions of the $|0\rangle$, $|1\rangle$, and $|S\rangle$ states, in which the shelving state is occupied for approximately 100 ps. The second AP step then completes the transfer.

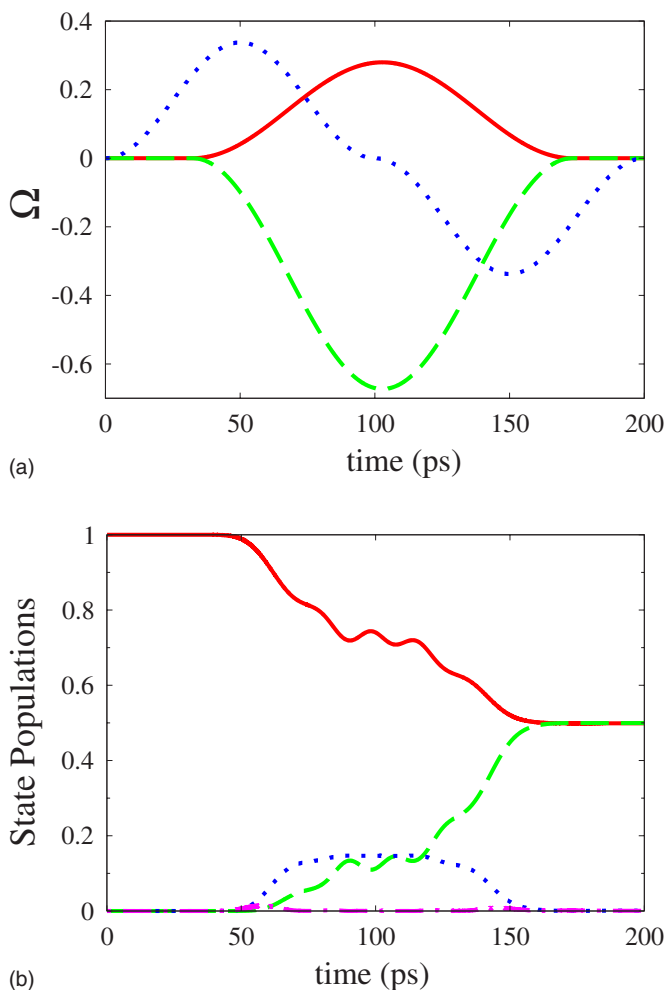


FIG. 3. (Color online) Calculations for the implementation of a Hadamard gate on our one-qubit system beginning in the state $|0\rangle$. Same units as in Fig. 2. (a) Temporal evolution of the three real valued Rabi frequencies of the pulses coupling each of the states to $|I\rangle$. Solid line: Ω_0 . Dashed line: Ω_1 . Dotted line: Ω_S . (b) The populations of the four states: $|0\rangle$ (solid line), $|1\rangle$ (dashed line), $|S\rangle$ (dotted line), and $|I\rangle$ (dot-dashed line), throughout the gate operation.

III. TWO-QUBIT GATES

We now consider an arbitrary two-qubit state given by

$$|\psi_0\rangle = \alpha_{00}|00\rangle + \alpha_{01}|01\rangle + \alpha_{10}|10\rangle + \alpha_{11}|11\rangle \quad (8)$$

normalized to unity. Similar to the one-qubit case we encode the four-qubit states and two additional states, $|I\rangle$ and $|S\rangle$, in six particular rovibrational eigenstates of our molecule. As before, $|I\rangle$ acts as the intermediate state, used to transfer population to and from the shelving state $|S\rangle$. The desired gate operation determines which states out of the four-qubit states gets coupled to the $|I\rangle$ state.

We present an explicit realization of a CNOT gate. The procedure developed here has obvious and immediate extensions to other two-qubit gate operations (such as the SWAP or controlled phase). Similarly, our method can be easily extended to three-qubit gate operations, such as the Toffoli (controlled-CNOT) gate. The pulse sequence of these composite gates thus generated is expected to be more efficient than

TABLE I. Input-output table for a quantum CNOT gate. The value of the second qubit, given on the right in the two-qubit ket notation, will be flipped only if the value of the first qubit is 1.

In	Out
$ 00\rangle$	$ 00\rangle$
$ 01\rangle$	$ 01\rangle$
$ 10\rangle$	$ 11\rangle$
$ 11\rangle$	$ 10\rangle$

the in tandem application of a sequence of the elementary gates.

A. Controlled-NOT gate

The CNOT gate acts by flipping the state of the second (or target) qubit only if the first (or control) qubit has a value of 1, depicted in Table I. After a CNOT gate operation, the initial two-qubit state of Eq. (8) transforms into

$$|\psi_f\rangle = \alpha_{00}|00\rangle + \alpha_{01}|01\rangle + \alpha_{11}|10\rangle + \alpha_{10}|11\rangle. \quad (9)$$

The implementation of this gate must therefore be able to achieve complete population transfer between the $|10\rangle$ and $|11\rangle$ states, without perturbing the coefficients of either the $|00\rangle$ or the $|01\rangle$ states. Because of the simple storage of qubits we have adopted, this task is reduced to simply exchanging the populations between two given rovibrational eigenstates within the same electronic manifold.

The use of a one-photon π -pulse scheme is precluded because of the requirement in that scheme that the pulse area be *exactly* equal to π to obtain satisfactory (i.e., near 100%) fidelity. Instead, we have devised a simple scheme capable of performing this operation using three APT processes (which are less sensitive to the pulse area) applied in tandem. The

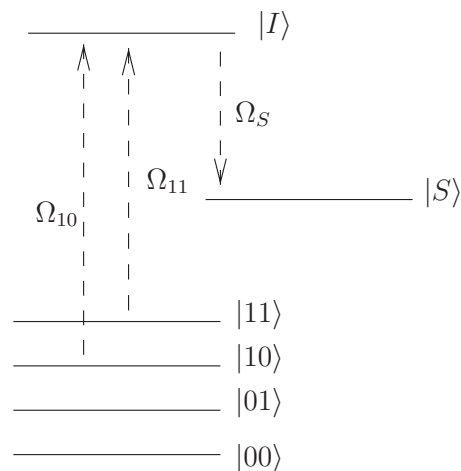


FIG. 4. Two-qubit interaction scheme for the implementation of the CNOT gate. Of the four states, $|00\rangle$, $|01\rangle$, $|10\rangle$, and $|11\rangle$, which encode the two qubits, only the latter two are involved in this operation. Similar to the one-qubit case, these states are coupled to the intermediate state $|I\rangle$, which in turn is coupled to the additional shelving state $|S\rangle$.

scheme, shown in Fig. 4, is similar to that used for the single qubit gates, with the three involved states coupling solely to the intermediate state $|I\rangle$. In the first stage one of the two upper qubit states, e.g., $|11\rangle$, undergoes an APT to the shelving eigenstate $|S\rangle$. As before, the pulses are applied in the “counterintuitive” order, first $\Omega_S(t)$ and then $\Omega_I(t)$, while maintaining a significant overlap between them. Once the $|11\rangle$ state has been emptied, we transfer the population from $|10\rangle$ to $|11\rangle$, using pulses whose Rabi frequencies are Ω_I and Ω_0 . Last, to complete the procedure, the shelved population in $|S\rangle$ is transferred to the (now) vacant $|10\rangle$ state.

Our scheme requires the use of only three laser frequencies, with the overall gate fidelity being determined solely by the efficiency of each APT step. An implementation to the two-qubit SWAP gate or to the three-qubit CCNOT gate follows essentially the same scheme, save for the employment of different assignments for the qubit states, e.g., $|01\rangle$, $|10\rangle$ for the SWAP gate and $|110\rangle$, $|111\rangle$ for the CCNOT gate.

1. CNOT gate operation

Using the same state representation as before, we encode our states in the following rovibrational levels of Na_2 : levels $|X, v=0, J=0\rangle$, $|X, v=2, J=0\rangle$, $|X, v=2, J=2\rangle$, $|X, v=4, J=2\rangle$ are used for the qubit basis states $|00\rangle$, $|01\rangle$, $|10\rangle$, and $|11\rangle$, respectively; then we use $|X, v=4, J=0\rangle$ for the shelving level and $|B, v=3, J=1\rangle$ as the intermediate state. In this case each level except the ground state $|00\rangle$ couples strongly to the excited level.

Such a simulation is shown in Fig. 5. We begin with an initial state given by

$$|\psi_i\rangle = \frac{1}{\sqrt{7}}(|00\rangle + |01\rangle - 2|10\rangle + |11\rangle). \quad (10)$$

We use the scaled Rabi frequencies shown in Fig. 5(a), which are now entirely real, and introduce in each of the three APT processes a relative Pump and Stokes phase difference of π in order to eliminate the extra π phase picked up by the target state due to the evolution [28]. The populations of the states throughout the gate operation are shown in Fig. 5(b). We see that the population of state $|11\rangle$ is first transferred and stored in $|S\rangle$ and then the population of state $|10\rangle$ is transferred completely to state $|11\rangle$. Finally the population of state $|S\rangle$ is transferred to state $|10\rangle$. We note that the shelving state $|S\rangle$ is occupied for less than 100 ps, well below the spontaneous emission decay time. Notice that due to unwanted coupling affects the intermediate state periodically collects population for several ps, however, this remains below the average cited decay time of such levels [35]. This affect also causes population leaking into the imaginary parts of the qubit coefficients, see Fig. 5(c).

As shown in the figure, the final state agrees exactly with the theoretically expectation of Sec. III A, i.e., with

$$|\psi_f\rangle = \frac{1}{\sqrt{7}}(|00\rangle + |01\rangle + |01\rangle - 2|11\rangle). \quad (11)$$

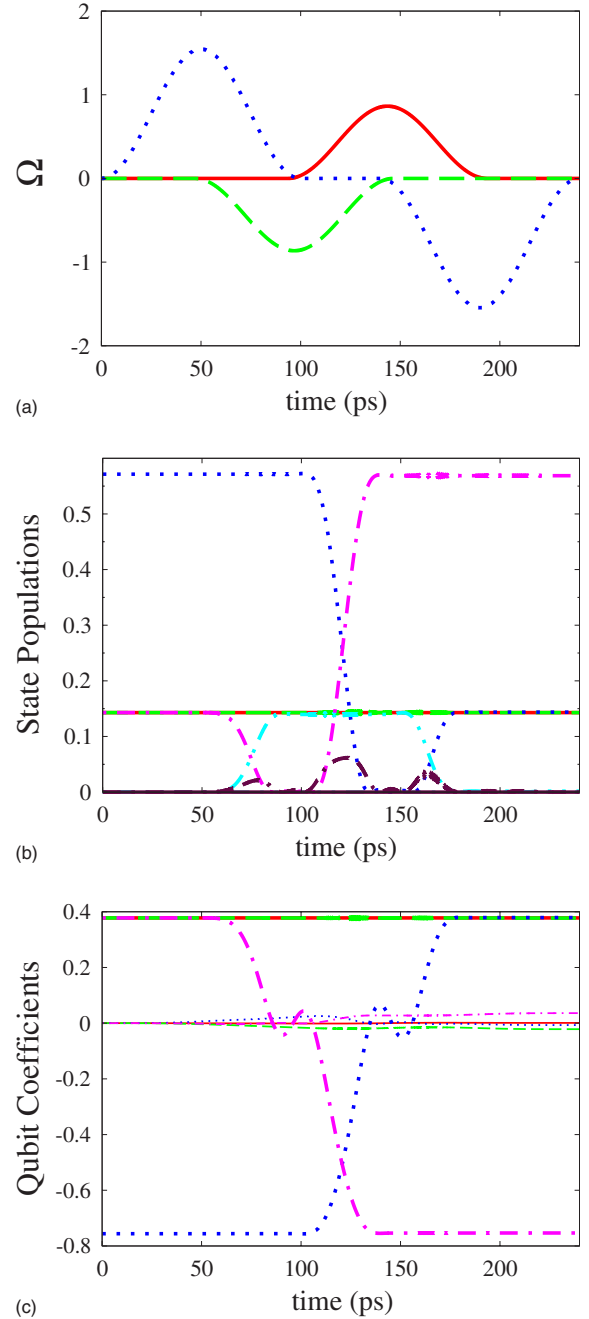


FIG. 5. (Color online) Numerical simulation of a CNOT gate implemented on a two-qubit system with an initial population split 1:1:2:1 between its four basis states. We use the same units as before. The same representation is used as in the previous plot. (a) Temporal profile of the Rabi frequencies of the pulses coupling each of the states to $|I\rangle$ for the three successive APT processes required to implement this gate. Solid line: Ω_{10} . Dashed line: Ω_{11} . Dotted line: Ω_S . (b) Time evolution of the populations of the six states throughout the gate operation. These states are represented as $|00\rangle$ (solid line), $|01\rangle$ (dashed line), $|10\rangle$ (dotted line), $|11\rangle$ (dot-dashed line), $|S\rangle$ (dash-dot-dot), and $|I\rangle$ (dash-dash-dot). The three independent APT processes between each of the states can be clearly seen. (c) The evolutions of the four qubit coefficients are shown using the same representation as in part (b). The thicker and thinner lines represent the real and imaginary parts of the coefficients.

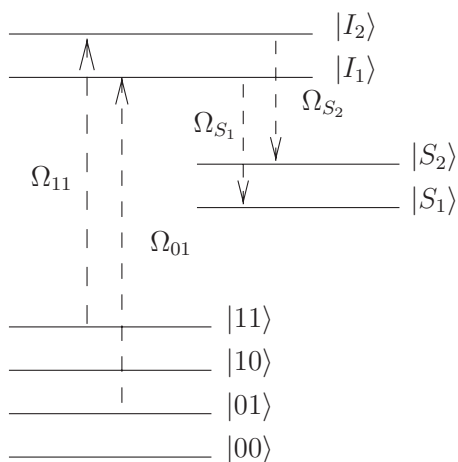


FIG. 6. Illustration of the pulses used for a one-qubit phase gate applied to the second (right) qubit in a two-qubit system. Since two one-qubit operations are being performed simultaneously, there are two intermediate, $|I_1\rangle$, $|I_2\rangle$, and two shelving, $|S_1\rangle$, $|S_2\rangle$, states in addition to the two-qubit basis states. Each of the two pulse envelopes contains two frequencies, $\{\Omega_{01}, \Omega_{11}\}$ and $\{\Omega_{S1}, \Omega_{S2}\}$, which address the appropriate levels for the two APT processes.

B. One-qubit gates of N -qubit numbers

In our encoding scheme, each of the possible combinations of qubits is assigned a single rovibrational level of a molecule. Therefore in order to perform a particular one-qubit gate on each qubit of all N -qubit numbers, we must carry out N of these one-qubit operations on each of the appropriately selected 2^N levels. For instance, suppose we wish to apply a one-qubit phase gate, defined as before, on the *second* (right) qubit represented in our two-qubit system. This action will take our initial state from Eq. (8) to a final state

$$|\psi_f\rangle = \alpha_{00}|00\rangle + \alpha_{01}e^{i\phi}|01\rangle + \alpha_{10}|10\rangle + \alpha_{11}e^{i\phi}|11\rangle. \quad (12)$$

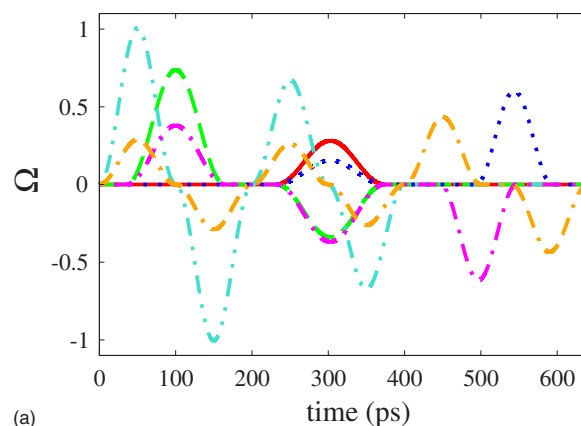
In this operation a phase ϕ has been added to each of the two two-qubit states whose *second* qubit is $|1\rangle$. If we had chosen the *first* qubit as the target then the $|10\rangle$ and the $|11\rangle$ states would have been multiplied by the $e^{i\phi}$ phase factor.

There are two basic options of implementing this and other one-qubit operations using our APT procedures in this two-qubit system:

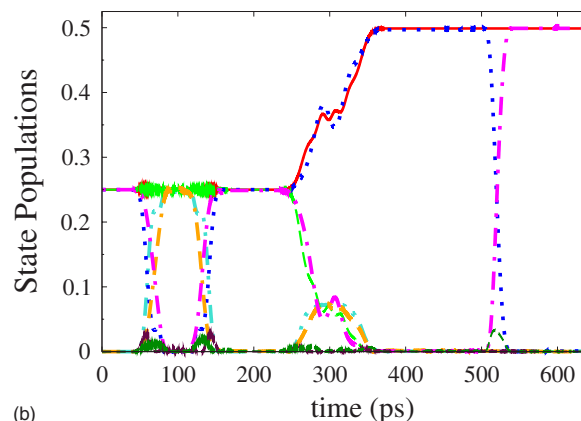
(i) One can perform two consecutive phase-gate operations for each of the two levels, using the same intermediate and shelving states for both processes.

(ii) One can introduce another intermediate and shelving state, $|I_2\rangle$ and $|S_2\rangle$, and then perform the two phase gates simultaneously on both qubit states, as shown in Fig. 6.

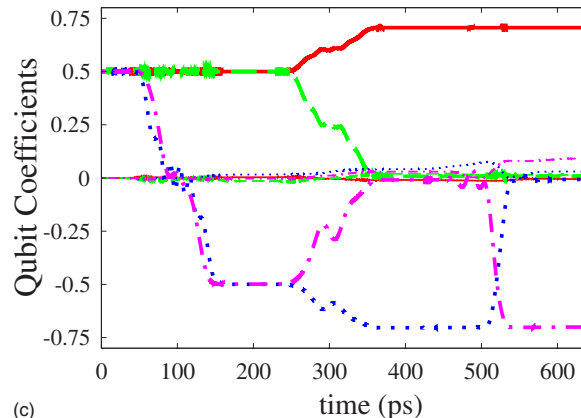
The second option would appear preferable because it would consume half (or an N th) the amount of time of the first option. However, it is more restricted: First, the laser pulses must be accurately constructed such that the appropriate levels are simultaneously coupled for each of the transitions, and second, the encoding of these states in the rovibrational eigenstates of the molecule must be chosen such that



(a)



(b)



(c)

FIG. 7. (Color online) Results from the numerical simulation of the three discussed gates, constituting a universal gate set, applied to our two-qubit system initialized to an even superposition of the four-qubit basis states. Two consecutive pulse sequences are applied to the appropriate levels to perform each of the two single qubit gate operations. The units used are as before. (a) Plot of the Rabi frequencies for the pulses coupling each one of the states: $|00\rangle$ (solid), $|01\rangle$ (dashed), and $|S_1\rangle$ (dash-dot-dot) to the intermediate state $|I_1\rangle$; and $|10\rangle$ (dotted), $|11\rangle$ (dash-dot), and $|S_2\rangle$ (dash-dash-dot) to $|I_2\rangle$. (b) Time evolution for each state's population. We use a similar representation as in Fig. 5(b) with changes to the state $|S_2\rangle$ (dash-dash-dot), and the two intermediate levels (thin solid lines) whose populations fluctuate near zero. (c) The evolutions of the four-qubit coefficients are shown using the same representation as before. The thicker and thinner lines represent the real and imaginary parts of the coefficients.

there is no interference between the two simultaneous processes. Thus if we are to perform two simultaneous one-qubit operations in a two-qubit system, each of the two laser pulses will have to contain two different Rabi frequencies tuned to be in resonance with the transitions depicted in Fig. 6. In this scheme we first apply the two pulses $\{\Omega_{S_1}, \Omega_{S_2}\}$ followed by the $\{\Omega_{01}, \Omega_{11}\}$ pair, thereby simultaneously transferring the populations of the $|10\rangle$ and $|11\rangle$ states to the two shelving levels, $|S_1\rangle$ and $|S_2\rangle$, respectively. Then, as before, this pulse sequence is reversed and the populations are sent back with the desired phase to their original levels.

In the N -qubit systems, N different narrow-band pulses must be contained within each pulse envelope in order to simultaneously perform the N single qubit operations. Experimentally, we can design such pulses using commercially available pulse shapers. The above strategy also applies to the Hadamard and other one-qubit gates.

C. Composite operations on two-qubit systems

We now apply our technique to perform composite operations made up of the phase-change, Hadamard, and CNOT logic gates on two-qubit systems, thereby proving its ability to perform any desired quantum computation on qubit systems of arbitrary dimensions. Instead of demonstrating again the $\pi/8$ phase (T) gate we study the π -phase change gate, which involves simply adding a different phase to one of the pulses in the second APT process, as discussed in Sec. II D. We show that one can produce in this way a molecular representation of a Bell state with essentially 100% fidelity. Here we use the same molecular state encoding as in the CNOT example, with the additional shelving ($|S_2\rangle$) and intermediate state ($|I_2\rangle$) encoded in the $|X, v=0, J=2\rangle$ and $|B, v=1, J=1\rangle$ states, respectively. In Fig. 7 we present simulations of three consecutive gate operations on a *product* initial state:

$$|\psi_i\rangle = \frac{1}{2}(|0_1\rangle + |1_1\rangle)(|0_2\rangle + |1_2\rangle) = (|00\rangle + |01\rangle + |10\rangle + |11\rangle). \quad (13)$$

The first operation performs a π -phase gate on the *first* (left) qubit if this qubit is 1, resulting in the state

$$|\psi_m\rangle = \frac{1}{2}(|00\rangle + |01\rangle - |10\rangle - |11\rangle). \quad (14)$$

The two individual phase-gate operations that must be performed on the $|01\rangle$ and $|11\rangle$ states are separated for demonstration. However, since these procedures can be done simultaneously by tuning the pulses to address each of the appropriate levels we used different intermediate, $|I_1\rangle$, $|I_2\rangle$, and shelving states, $|S_1\rangle$, $|S_2\rangle$, for each case.

In the next step a Hadamard gate acts on the second (right) qubit of $|\psi_m\rangle$. Shown in Fig. 7(a) are the two consecutive single qubit processes: $|00\rangle + |01\rangle \rightarrow |00\rangle$ and $-(|10\rangle + |11\rangle) \rightarrow -|10\rangle$ that together give us the state

$$|\psi_n\rangle = \frac{1}{\sqrt{2}}(|00\rangle - |10\rangle). \quad (15)$$

Finally, we apply a CNOT gate, moving the population from $|10\rangle$ to $|11\rangle$. Since the target state did not contain any population, the shelving state was not required. (In fact a basic three-level APT transfer scheme would have been sufficient.) The final operation leaves us in a representation of a Bell state,

$$|\psi_f\rangle = \frac{1}{\sqrt{2}}(|00\rangle - |11\rangle). \quad (16)$$

This combined logic operation is characterized by the same essentially perfect gate fidelity encountered for each of the individual gates. A calculation finds an error of less than 0.01% for this process, the slight deviation from previously higher stated fidelities are due to the large variations in Rabi frequencies between pulses that we use in order to test the robustness of the scheme. Higher accuracy, approaching the presumed fault-tolerant error threshold of 99.99%, can be obtained by minor tuning of the pulses' intensities together with an additional lengthening of the pulses conjoining each of the consecutive APT processes.

IV. CONCLUSIONS

We have developed a method of implementing a universal gate set on one- and two-qubit molecular systems using APT. We have demonstrated the procedure using the Na_2 -molecule vibrational states. Our method is robust and produces nearly flawless gate fidelities. The procedure can be readily extended to perform any quantum computation on much larger systems. An experimental realization of our procedure in the Na_2 molecule is now being developed.

We have shown that when the number of qubits is increased it is possible to shorten the performance times by using more molecular levels. Although this shortening of performance times uses more resources (molecular levels), it enables *multiplexing* and saving in *laser* resources, because the procedure then uses fewer pulses, with each pulse being composed of many narrow-band components. Such pulses can now be readily prepared using commercially available pulse shapers.

Although we have shown how to produce a molecular representation of a Bell state, we have so far not *exploited* the theoretically predicted superior scaling of entangled states. In molecular systems, entanglement of the vibrational and the rotational quantum states in an ordinary optical excitation process is easily attainable via broadband excitations from a $|v_i\rangle|J_i\rangle$ initial state to produce an entangled superposition of energetically close $|v'\rangle|J_i+1\rangle$ and $|v'\rangle|J_i-1\rangle$ states. The exploitation of such entanglements in conjunction with our procedures is now being investigated.

ACKNOWLEDGMENTS

We thank Evgeny Shapiro and Ioannis Thanopoulos for invaluable discussions.

- [1] M. A. Nielson and I. L. Chuang, *Quantum Computation and Quantum Information* (Cambridge University Press, Cambridge, England, 2000).
- [2] J. P. Palao and R. Kosloff, Phys. Rev. Lett. **89**, 188301 (2002).
- [3] J. P. Palao and R. Kosloff, Phys. Rev. A **68**, 062308 (2003); **69**, 059901(E) (2004).
- [4] U. Trumann, C. Tesch, and R. de Vivie-Riedle, Chem. Phys. Lett. **378**, 273 (2003).
- [5] D. Babikov, J. Chem. Phys. **121**, 7577 (2004).
- [6] C. Tesch and R. de Vivie-Riedle, J. Chem. Phys. **121**, 12158 (2004).
- [7] U. Troppman and R. de Vivie-Riedle, J. Chem. Phys. **122**, 154105 (2005).
- [8] S. Rice and M. Zhao, *Optical Control of Molecular Dynamics* (Wiley-Interscience, New York, 2000).
- [9] D. Tannor and S. Rice, J. Chem. Phys. **83**, 5013 (1985).
- [10] S. Shi, A. Woody, and H. Rabitz, J. Chem. Phys. **88**, 6870 (1988).
- [11] E. Farhi *et al.*, Science **292**, 472 (2001).
- [12] W. Kaminsky, S. Lloyd, and T. Orlando, e-print arXiv:quant-ph/0403090v2.
- [13] M. Steffen, W. vanDam, T. Hogg, G. Breyta, and I. Chuang, Phys. Rev. Lett. **90**, 067903 (2003).
- [14] M. Grajcar, A. Izmailkov, and E. Il'ichev, Phys. Rev. B **71**, 144501 (2005).
- [15] M. S. Sarandy and D. A. Lidar, Phys. Rev. Lett. **95**, 250503 (2005).
- [16] A. M. Childs, E. Farhi, and J. Preskill, Phys. Rev. A **65**, 012322 (2001).
- [17] P. Zanardi and M. Rasetti, Phys. Lett. A **264**, 94 (1999).
- [18] A. M. Samoilenko, Y. A. Prykarpatsky, U. Taneri, A. K. Prykarpatsky, and D. L. Blackmore, Math. Comput. Simul. **66**, 1 (2004).
- [19] D. Lucarelli, J. Math. Phys. **46**, 052103 (2005).
- [20] L.-A. Wu, P. Zanardi, and D. A. Lidar, Phys. Rev. Lett. **95**, 130501 (2005).
- [21] U. Gaubatz, P. Rudecki, S. Schiemann, and K. Bergmann, J. Chem. Phys. **92**, 5363 (1990).
- [22] K. Bergmann, H. Theuer, and B. Shore, Rev. Mod. Phys. **70**, 1003 (1998).
- [23] Z. Kis and F. Renzoni, Phys. Rev. A **65**, 032318 (2002).
- [24] H. Goto and K. Ichimura, Phys. Rev. A **70**, 012305 (2004).
- [25] N. Sangouard, X. Lacour, S. Guérin, and H. Jauslin, Eur. Phys. J. D **37**, 451 (2006).
- [26] N. Sangouard, X. Lacour, S. Guérin, and H. R. Jauslin, Phys. Rev. A **72**, 062309 (2005).
- [27] N. Vitanov, M. Fleischhauer, B. Shore, and K. Bergmann, Adv. At., Mol., Opt. Phys. **46**, 55 (2001).
- [28] M. Shapiro and P. Brumer, *Principles of the Quantum Control of Molecular Processes* (John Wiley and Sons, Inc., Hoboken, NJ, 2003).
- [29] V. Hughes and L. Grabner, Phys. Rev. **79**, 829 (1950).
- [30] W. J. Stevens *et al.*, J. Chem. Phys. **66**, 1477 (1977).
- [31] K. Xu, T. Mukaiyama, J. R. Abo-Shaeer, J. K. Chin, D. E. Miller, and W. Ketterle, Phys. Rev. Lett. **91**, 210402 (2003).
- [32] F. K. Fatemi, K. M. Jones, P. D. Lett, and E. Tiesi, Phys. Rev. A **66**, 053401 (2002).
- [33] P. Boykin, T. Mor, M. Pulver, V. Roychowdhury, and F. Vatan, Inf. Process. Lett. **75**(3), 101 (2000).
- [34] W. Demtröder, W. Stetzenback, M. Stock, and J. Witt, J. Mol. Spectrosc. **61**, 382 (1976).
- [35] J. J. Camacho, A. Pardo, and J. M. L. Poyato, J. Phys. B **38**, 1935 (2005).
- [36] R. G. Unanyan, B. W. Shore, and K. Bergmann, Phys. Rev. A **59**, 2910 (1999).